Single-Fiber Sagnac-Like Interferometer for Optical Rotation Measurement in Atomic Spin Precession Detection

Xuejing Liu, Yuanhong Yang, Ming Ding, Wei Quan, Yanhui Hu, Yang Li, Wei Jin, and Jiancheng Fang

***Abstract*—In this paper, a single-fiber Sagnac-like interferometer is proposed and experimentally demonstrated for detecting atomic spin precession in an atomic magnetometer. The single-fiber Sagnac-like interferometer has a reciprocal optical structure, which is insensitive to environmental disturbances. The fiber system is more flexible for implementation in miniature atomic magnetometers, which has potential for application in magnetoencephalography systems. The sensitivity and the bandwidth of the system are also discussed. The thermal and bending disturbances to fiber system are observed, whereas the long-term stability is analyzed and compared with the Faraday modulation scheme.**

***Index Terms*—Atomic magnetometer, fiber Sagnac-like interferometer, Larmor precession, spin exchange relaxation free, spin precession detection.**

I. Introduction

OPTICAL rotation is the rotation of polarization plane of linearly polarized light as it travels through certain materials [1]. The measurement of optical rotation has been of great interest due to its usefulness for concentration calculations [2]. Additionally, many sensors are designed using the effect of optical rotation [3]. Among them, atomic magnetometers [4] with ultra-high sensitivity have brought about new challenges for measuring optical rotation [5]. An atomic magnetometer is based on the atomic Larmor precession in magnetic fields [6]. The essential of precession detection is the measurement of optical rotation. The sensitivity of atomic magnetometer has reached 0.16 fT/Hz$^{1/2}$ with gradient measurement [7], which is equivalent to an extremely small optical rotation of the magnitude of 1.6×10^{-8} rad/Hz$^{1/2}$ [8].

Manuscript received xxxx, 2018; revised xxxx, 2018; accepted xxxx, 2018. Date of publication xxxx, 2018 *(Corresponding author: Ming Ding.)*

X. Liu, Y. Yang, Y. Hu, Y. Li, W. Jin, and J. Fang are with the School of Instrumentation Science and Opto-electronics Engineering, Beihang University, Beijing 100191, China (e-mail: liuxuejing@outlook.com; yhyang@buaa.edu.cn; huyanhui1110@sina.com; liy_db@163.com; wei.jin@polyu.edu.hk; fangjiancheng@buaa.edu.cn).

M. Ding and W. Quan are with the School of Instrumentation Science and Opto-electronics Engineering, Key Laboratory of Ministry of Industry and Information Technology on Quantum Sensing Technology, Beijing Advanced Innovation Center for Big Date-based Precision Medicine, Beihang University, Beijing 100191, China (e-mail: mingding@buaa.edu.cn; quanwei@buaa.edu.cn).

The conventional methods consist of polarimetric detection techniques [9]. Initial work on spin precession detection used an off-resonance laser with a well-defined linear polarization, and analyzed its polarization state after passing through the vapors [10]. Then, a Faraday modulator was employed for isolating the noise at low frequency. The magnetic field sensitivity of 7 fT/Hz$^{1/2}$ was achieved using the Faraday modulation scheme, which was equivalent to an optical rotation of 7×10^{-7} rad/Hz$^{1/2}$ [11].

In 2006, the atomic magnetometer was first applied to magnetoencephalography (MEG) system due to the advantage that it did not require use of helium [12]. Since then, minimization of atomic magnetometer has attracted large attentions to make an array of sensors, which can be installed within a helmet [13]. Therefore, the performance of magnetometers has been compromised due to miniaturization, which means that the sensitivity and measurement range of 10^{-6} rad/Hz$^{1/2}$ and 10^{-7}–10^{-5} rad were expected [14]. However, all the optical components can hardly be stabilized due to thermal and vibrations fluctuations, especially for compact systems [15]. In 2018, Quspin Inc., USA. pushed out a commercial atomic magnetometer with the sensitivity of 10 fT/Hz$^{1/2}$ and the drift of 2 pT/h, which was equivalent to 2×10^{-4} rad/h [16]. Therefore, a compact system with higher stability for atomic spin precession detection has been urgently desired.

Fiber sensors have the advantages of low-cost and being immune to electrical interference [17]–[21], which are widely applied in industrial areas. For the measurement of optical rotation, the applications of fiber polarimetric sensors are limited due to changes in birefringence of fibers caused by the environment [22]. In 1996, James Blake utilized fiber Sagnac interferometer to measure current based on the Faraday effect of the fiber with a resolution of a few microradians and successfully applied the interferometer in electric power industry [23]. With the advantages of reciprocal light path, the sensors are insensitive to disturbance caused by the environment.

Herein, the use of a single-fiber Sagnac-like interferometer is reported for detecting atomic spin precession in an atomic magnetometer. The interferometer has the potential to be applied in remote magnetic sensing for MEG systems. In this case, vapor cell subjected to magnetic fields generates the phase shift measured by the interferometer. Two lights with the reciprocal light path configuration are used to measure the phase shift when both beams of light pass through the vapor cell. This system

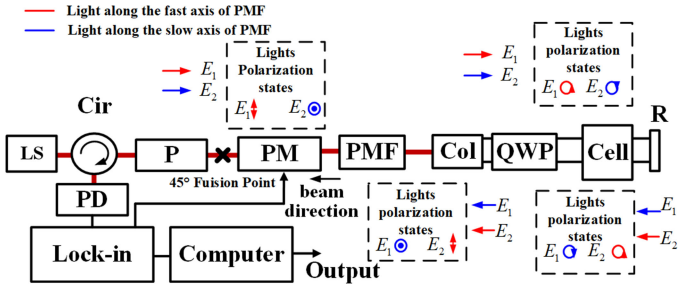

Fig. 1. Single-fiber Sagnac-like interferometer system for atomic spin precession detection. LS: light source; Cir: circulator; P: polarizer; PM: phase modulator; PMF: polarization maintaining fiber; Col: collimator; QWP: quarter waveplate; R: reflector; PD: photodetector; Lock-in: lock-in amplifier. E_1 and E_2 are the orthogonal components, which are aligned to the principal axes of PM; E_s and E_f represent the polarization states along fast and slow axes of PMF; E_l and E_r represent the left and right circularly polarization states of beams in the vapor cell.

operates in a reflection mode, thus enabling the single lead in/out fiber to atomic vapor cell and making it flexible to be assembled and miniaturized. With such a system, the vapor cell can be separated from other optical and electrical elements, minimizing the volume of bulky optical components, and enhancing the spatial resolution of MEG headers. Moreover, this single-fiber Sagnac-like interferometer has a reciprocal light path structure, which is insensitive to environmental disturbances.

The principles of single-fiber Sagnac-like interferometer for atomic spin precession detection are described in Section II. The experimental setup and the preliminary results are presented in Sections III and IV, respectively.

II. Principle

Fig. 1 shows the single-fiber Sagnac-like interferometer system for detecting atomic spin precession. The fiber circulator (Cir) is used to direct the light from a probe laser source (LS) to a polarizer (P). The resulting linearly polarized light has a 45° angle with respective to the polarization principal axes (x and y) of the phase modulator (PM), which results in equal splitting of light power along x and y axes of the PM. Herein, these two orthogonally polarized light beams are denoted as E_1 and E_2. E_1 and E_2 pass through the PM for the first time at $t-\tau$. Their phases are modulated as $\Phi_1(t-\tau)$ and $\Phi_2(t-\tau)$, respectively, where τ is the round trip propagation delay of light through the system. After PM, the two beams propagate along the slow (E_s) and fast (E_f) axes of the polarization maintaining fiber (PMF) to a fiber collimator (Col), are converted into left (E_l) and right (E_r) circularly polarized light beams respectively through quarter wave-plate (QWP), and then, pass through the alkali vapor cell. As the pumped cell after QWP is a circular birefringence medium, the left and right circular polarization beams propagate at different velocities, and experience a phase difference $\Delta\phi$, which can be described using optical rotation θ as: $\Delta\phi = 2\theta$. After reflection by the reflector (R), the left and right circular polarization beams switch directions, become linearly polarized again after passing through QWP, and then, propagate in the PMF as E_f and E_s. The QWP and R act together as a reflective half waveplate (HWP), which rotates the linear polarization of E_1 and E_2 with an angle of 90° [24]. These two orthogonal beams propagate backwards along the same path, and pass through the PM for the second time at t. They are coherently mixed at the polarizer P, whereas the output interfering intensity is detected using a photodetector (PD) after the Cir. The output is demodulated using a lock-in amplifier.

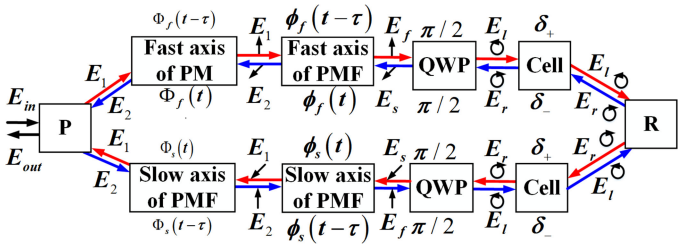

Fig. 2. Reciprocity of the fiber Sagnac interferometer for atomic spin precession detection; ϕ_s and ϕ_f are the PMF phase delays in slow and fast axes, whereas Φ_s and Φ_f are the PM phase delays in slow and fast axes, respectively.

Practically, the fiber is sensitive to environment, especially for thermal and vibration disturbances. However, the reciprocity of single-fiber Sagnac-like interferometer cancels most of the disturbances, and hence, makes the system more suitable for engineering applications. Fig. 2 shows the reciprocal optical paths of the two orthogonal light beams propagating in single-fiber Sagnac-like interferometer system. The beams E_1 and E_2 for spin precession detection are generated after passing through the 45° splice between P and PM. The changes in polarization states of the two beams at various optical elements are shown in Fig. 2. The changes in phase retardation of E_1 are labelled on the element block and are produced by each optical element. On the other hand, those of E_2 are labelled under the element block. $\Phi_s(t)$ and $\Phi_f(t)$ are the phase delays experienced by the two orthogonal polarization states in PM at different time intervals. Furthermore, $\phi_s(t)$ and $\phi_f(t)$ are the phase delays experienced by the two orthogonal polarization states in PMF, which contain the disturbances in the environment at different time intervals. Additionally, δ_+ and δ_- represent the phase retardations experienced by E_l and E_r respectively, when they pass through the alkali vapor cell.

The total phase retardation φ_1 of beam E_1 is given:

$$\varphi_1 = \phi_f(t-\tau) + \phi_s(t) + 2\delta_+ + \Phi_s(t-\tau) + \Phi_f(t) \quad (1)$$

The total phase retardation φ_2 of beam E_2 is expressed as:

$$\varphi_2 = \phi_s(t-\tau) + \phi_f(t) + 2\delta_- + \Phi_f(t-\tau) + \Phi_s(t) \quad (2)$$

The two beams are brought back together and interfered by the common input/output polarizer. Finally, they are coupled to the detector. The phase difference $\Delta\varphi$ between E_1 and E_2 is given by:

$$\begin{aligned}\Delta\varphi &= \varphi_1 - \varphi_2 = 2(\delta_+ - \delta_-) - \Delta\Phi(t) + \Delta\Phi(t-\tau) \\ &= 4\theta - \Delta\Phi(t) + \Delta\Phi(t-\tau) \end{aligned} \quad (3)$$

where $\Delta\Phi(t) = a\sin\omega t$ and a is the amplitude of the differential phase modulation of PM.

According to Eq. (3), if the disturbances caused by the environment are reciprocal, the common phase retardation caused

by the optical elements and environmental disturbances is eliminated, thus benefiting from the reciprocity of light path. The phase difference between E_1 and E_2 depends only on the optical rotations occurring in the cell and the differential phase modulation in PM. Furthermore, the operation in the reflection mode doubles the optical path through vapor cell, and therefore, doubles the optical rotations of the vapor cell.

However, the cancellation of environmental disturbance is not complete in non-ideal environments. The time-varying disturbances, which alter birefringence of the PMF, affect the counter-propagating waves differently. Both the E_1 and E_2 experience the axis dependent perturbations at different time intervals, which can be regard as the error of optical rotation as given by Equation (4) provided in a previous work [23].

$$\theta_e = \frac{\pi n_f l L_m}{c L_B^2} \frac{\partial L_B}{\partial t} \tag{4}$$

where $n_f = 1.46$ is the refractive index of the fiber, l is the length of the fiber being perturbed, L_m is the distance between the perturbation point and the reflector, L_B is the polarization beat length of PMF and c is the velocity of light in free space. According to Eq. (4), the error is linearly correlated with the time rate of change of polarization beat length L_B, as well as with L_m. If the error is limited to 1 fT for atomic magnetometer, the length of fiber with $L_B = 1.8$ mm, should be less than 620 m.

The output of the interferometer system as detected at PD can be expressed as:

$$\begin{aligned} I_{out} &= \frac{1}{2} I_0 \left[1 + \cos\left(\Delta\varphi\right)\right] \\ &= \frac{1}{2} I_0 \left\{1 + \cos\left[4\theta - \Delta\Phi\left(t\right) + \Delta\Phi\left(t - \tau\right)\right]\right\} \end{aligned} \tag{5}$$

I_{out} contains DC and harmonic components of the signal, and the first harmonic component is given by:

$$I_{out} = K I_0 J_1\left(2a \sin\left(\omega\tau/2\right)\right) \sin\left(4\theta\right) \tag{6}$$

where K is the scale factor of PD, and I_0 is the input light intensity of the probe beam.

According to Eq. (6), the first harmonic component of the single-fiber Sagnac-like interferometer output can be treated as proportional to the optical rotation θ, provided the optical rotation is small (such that sin $\theta \sim \theta$).

According to Faraday effect, the environmental magnetic field rotates the polarization state of the probe light with an angle of ϑ, which is equivalent to the cross-talk between the fast and slow axes of polarization maintaining fiber (PMF). In order to evaluate this influence, an error model using Jones matrix is established.

Assuming the environmental magnetic field is uniform, for fiber system with 500 m PMF, the polarization rotation generated by the magnetic field is denoted as ϑ. Using the Jones matrix method [25], the output intensity of the system is described as:

$$\begin{aligned} I_{out} = &\frac{1}{2} + \frac{1}{2} \cos 4\theta \cos\left(\Delta\Phi\left(t - \tau\right) - \Delta\Phi\left(t\right)\right) \\ &- \frac{1}{2} \sin 4\theta \cos 2\vartheta \sin\left(\Delta\Phi\left(t - \tau\right) - \Delta\Phi\left(t\right)\right) \end{aligned} \tag{7}$$

The series expansion of the output is given by:

$$\begin{aligned} I_{out} = &\frac{1}{2} + \frac{1}{2} \cos 4\theta J_0\left[2a \sin\left(\tau/2\right)\right] \\ &+ \cos 4\theta \sum_{n=1}^{\infty} (-1)^n J_{2n}[2a \sin\left(\tau/2\right)] \cos\left[2n(\omega t - \tau/2)\right] \\ &+ \sin 4\theta \cos 2\vartheta \sum_{n=1}^{\infty} (-1)^n J_{2n-1}\left[2a \sin\left(\tau/2\right)\right] \\ &\times \cos\left[\left(2n-1\right)\left(\omega t - \tau/2\right)\right] \end{aligned} \tag{8}$$

According to Eq. (8), the environmental magnetic field changes the scale factor of the system with only odd harmonics. This is due to the reason that the system is more sensitive to circular birefringence, however less sensitive to linear birefringence. Referring to 0.0001 rad/m rotation in PMF [26], the rotation generated by the environmental magnetic field is about 0.1 rad, which has an error of 0.56% in the scale factor. If 1 fT signal is detected, there is an error signal having the magnitude of 5.6 aT, which is acceptable for environmental magnetic field.

The same condition is analyzed in the polarization differential detection scheme [4]. Under ideal conditions, the optical rotation of atomic spin precession is θ, whereas the output of the polarization differential detection is described as:

$$I = \frac{1}{2} \sin 2\theta \tag{9}$$

If the environmental magnetic field rotates the polarization state of the probe light with an angle of ϑ due to Faraday effect of the optical elements, the output of the system is modified and is given by:

$$I = \frac{1}{2} \sin\left(2\theta + 2\vartheta\right) \tag{10}$$

Compared to Eq. (8), this error is directly superimposed onto the signal, which is critical to weak optical rotation signal that lies within the range of 10^{-5}–10^{-7} rad.

The atomic magnetometer is based on the detection of polarized atomic spin precession in a magnetic field. The basic theory of atomic magnetometer has been described in a previous work [27]. The main points with respect to the detection of atomic spin precession are summarized as follows.

As shown in Fig. 3, a circularly polarized pump laser beam propagates in the z direction and passes through a vapor cell. It polarizes the atoms, generating atomic spin polarization $\vec{P}$. When an off-resonance, linearly polarized laser, passes through the vapor along the *x*-direction, the optical rotation θ is generated. When a magnetic field is applied, for example in *y* direction, the atomic spin $\vec{P}$ generates precession. The *x*-component (P_x) of the spin polarization is proportional to magnetic field B_y under weak magnetic field approximation [28] and the angle of rotation θ is proportional to P_x [29]. The magnetic field can then be detected through the rotation angle θ.

The atomic magnetometer seems ideal for biomagnetic imaging, particularly for recording the electromagnetic activity in brain. Optical-pumping magnetometers have successfully been used in the past to map the activity of heart, which produces

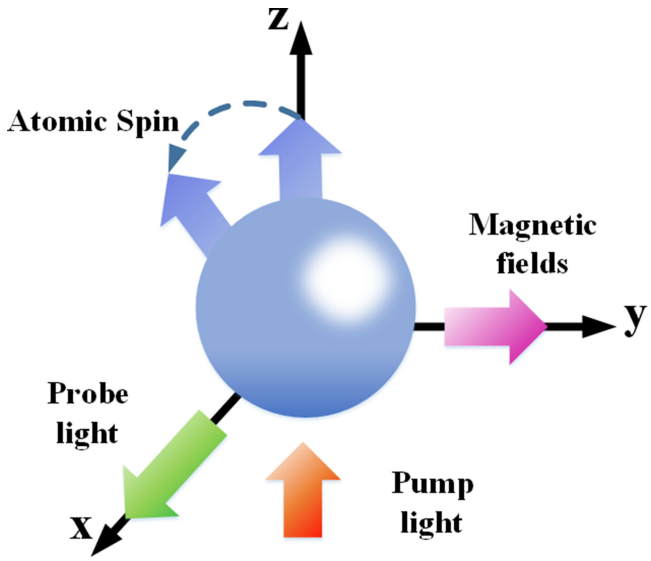

Fig. 3. Basics of an atomic magnetometer.

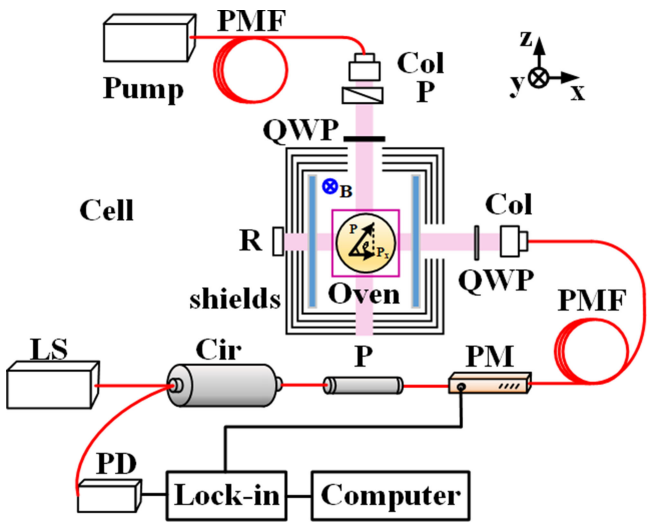

Fig. 4. Schematic of the spin exchange relaxation free (SERF) atomic magnetometer.

fields of the order of 10^{-10} T. However, brain imaging is at least a thousand times weaker [30], which means that the sensitivity of the fiber spin precession detection system should be better than 10^{-5} rad/Hz$^{1/2}$.

III. Experimental Setup and Procedure

The feasibility of the single-fiber Sagnac-like interferometer for detecting atomic spin precession is experimentally investigated. The single-fiber Sagnac-like interferometer is integrated into a spin exchange relaxation free (SERF) atomic magnetometer as the probe light path. SERF is an operating regime of alkali atomic vapor with high density and near zero magnetic field in the atomic magnetometer. Working in this regime, the spin exchange relaxation of the atomic vapor can be suppressed [27] and the sensitivity of atomic magnetometer can be improved significantly [31]. The schematic of the experimental setup is shown in Fig. 4. The sensitive unit of the atomic magnetometer is a 2 cm $\times$ 2 cm $\times$ 2 cm glass cell containing a small drop of potassium (K), 60 Torr of nitrogen (N_2), and 3 atm of helium (He) buffer gas. An electronic AC current heater is used to heat the cell to 473 K, at which point, the saturated K vapor concentration is about 7.1×10^{16} cm^{-3}.

The K atoms are spin-polarized by the pump laser, which has the power of 9 mW at $\lambda = 770$ nm and is centered at D1 line along the z direction. The laser is produced by an external cavity diode laser (ECDL) (model 6910, New Focus, USA). The laser output is circularly polarized by passing it through a polarizer and QWP with a cross angle of 45° between their optical axes.

The probe beam is generated using a DBR laser (TL100, Toptica) with a wavelength of $\lambda \approx 767$ nm, which is detuned to 2 GHz from D2 line of K. The line-width and the power level of DBR laser are 1 MHz and 20 mW, respectively. After passing through the fiber circulator (VCIR-3-766-L-10-FA, Ascentta) with an isolation of 28 dB, the laser is linearly polarized using a fiber polarizer (LPT-780), which has a central operating wavelength of 766.9 nm, a wavelength range of $\pm$50 nm, the insertion loss of 0.7 dB, and the extinction ratio of 28 dB. The polarization of the probe beam is modulated using the phase modulator (PM-0S5-10-PFU-PFU- 766/795, EOSpace Inc., USA) with 7.8 V @ 106 kHz half-wave retardation voltage. The probe beam is then delivered to the alkali atomic cell using a PMF and a collimator. The PMF (PM630-HP, Nufern) has a mode field diameter (MFD) of 4.5 $\pm$ 0.5 μm at $\lambda = 630$ nm and the birefringence of 3.5×10^{-4}, which is equivalent to a beat length $L_B = 1.8$ mm. Additionally, the collimator (PAF-X-15-PC-B, Thorlabs) has a focal length of 15.4 mm, which produces a light spot with a diameter of 3 mm. After the cell, the light was reflected using the reflector (BB1-E01, Thorlabs), which has dielectric mirror coatings with operational wavelength lying within the range of 750–1100 nm. The output signal is detected using a PD. The atomic spin precession signal is extracted from the first harmonic at the modulation frequency of 106 kHz using a lock-in amplifier (HF2LI, National Instruments).

As the magnetometer operates in a near-zero magnetic field, the ambient magnetic field should be nullified to avoid the broadening of resonance line-width. A set of four-layer μ-metal magnetic shields is mounted outside the cell assembly to isolate the geomagnetic field. In order to optimize the operation of atomic magnetometer, all three magnetic field components are further reduced to within 10 pT using tri-axial coils according to a cross-modulation technique [32], [33]. The magnetometer is calibrated by applying known magnetic fields. The response to calibration signal is detected using the PD and analyzed using the lock-in amplifier. The lock-in output is acquired using a computer equipped with the DAQ Card (Data Acquisition Card USB-6366, Zurich Instruments). The sampling rate is 1000/s and the sampling time is 100 s.

IV. Results and Discussion

Fig. 5 shows the frequency spectrum of lock-in output with (line in black) and without (line in red) the application of oscillating magnetic field $B_y = B_1 \cos \omega t$ along y-axis. The

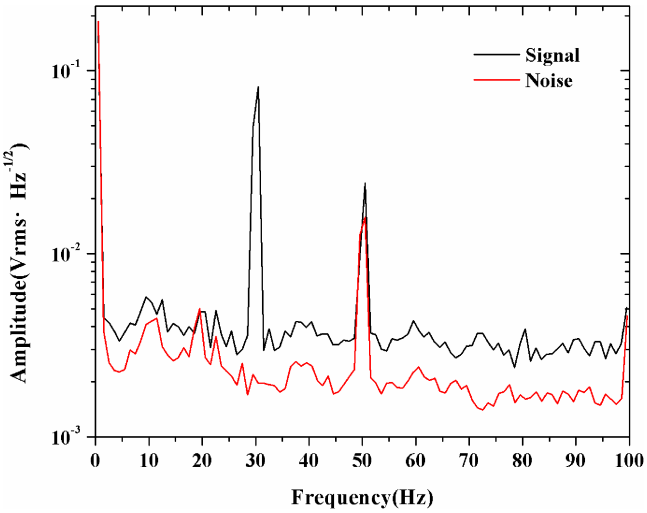

Fig. 5. Frequency spectrum of the single-fiber Sagnac-like interferometer. The line in black is the signal and the red is the noise measured without calibration signal in the atomic magnetometer.

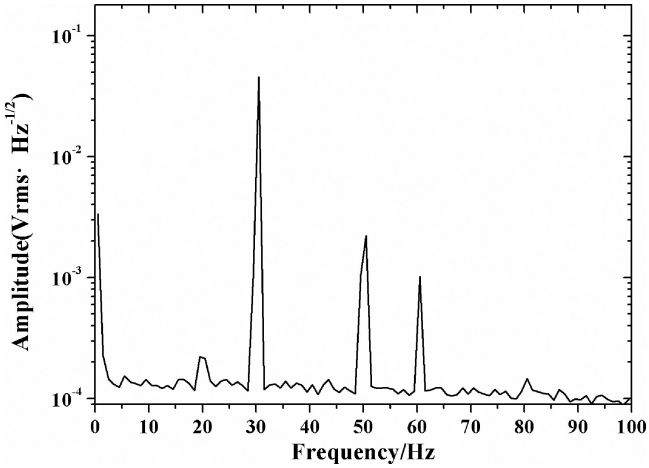

Fig. 6. The frequency spectrum of a SERF atomic magnetometer with the single-fiber Sagnac-like interferometer.

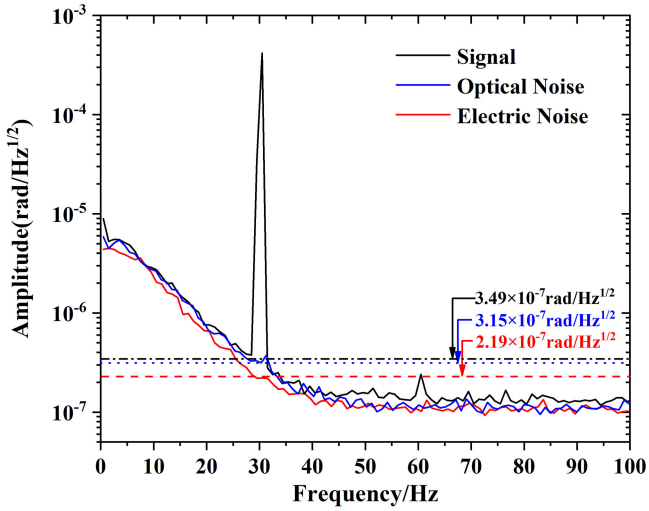

Fig. 7. The calibration and different noise of the single-fiber Sagnac-like interferometer. The blue line is for optical noise and the red one is for the electric noise.

magnetic field is generated from a series of Helmholtz coils, and has a calibrated magnitude of 86.3 pT at the frequency of 30 Hz. As shown in Fig. 5, the peak at 30 Hz represents the signal of atomic spin precession, which disappears when the oscillating field is removed. The peak at 50 Hz represents the industrial frequency signal as it is independent of the calibrated magnetic signal. By comparing the signal with the noise level around 30 Hz, the detection sensitivity in terms of noise equivalent magnetic field is estimated to be 11.1 pT/Hz$^{1/2}$.

This level of noise corresponds to about 10^{-5} rad/Hz$^{1/2}$ in terms of noise equivalent phase modulation. The relatively large noise is attributed to coherent back reflection at various optical interfaces. As shown in Fig. 4, multiple glass/air interfaces exist, whereas the long coherence length of the probe laser source means the reflected waves would interference coherently with the main signal beam and cause noise.

Furthermore, experiments were conducted using the same experimental system, but replacing the probe laser source with a low coherence super-radiance light emitting diode (SLD) (SLD-331, Superlum). The power of SLD is 20 mW and the wavelength range is 740–850 nm. The measurement conditions are the same as those used in the laser source and the corresponding results are shown in Fig. 6. The noise level is much lower, whereas the noise equivalent magnetic field is estimated to be 2.6 pT/Hz$^{1/2}$.

It should be mentioned that the use of broadband source also reduces the detected spin precession signal. This is due to the reason that the line-width of SLD is much broader than the laser source, and the detected signal is the integration of spin processing over the entire wavelength range of SLD. Spectral intensity of the probe beam around D1 and D2 lines of K atoms is much smaller, and results in a smaller detected signal. The performance of the system could be improved by optimizing the line-width and center wavelength of the probe beam (such as, to use a filter with center wavelength close to the D1 or D2 line and a narrower spectral width). On the other hand, as the laser has a higher calibration factor, the laser source could be considered in the premises of backscatter noise, which is being greatly reduced. The incidental phase modulation method [34] used in optical gyroscopes may improve the sensitivity of fiber system using a laser source, which is due to the reason that the noise could be averaged out efficiently within an appropriate time of observation.

The optical and electronic noises of the single-fiber Sagnac-like interferometer are analyzed and shown in Fig. 7. The fiber system is calibrated using a 4.2×10^{-4} rad @ 30 Hz optical rotation. The sensitivity of the system is about 3.49×10^{-7} rad/Hz$^{1/2}$, which is equivalent to 3.49 fT/Hz$^{1/2}$ for atomic magnetometer. The results show that the single-fiber Sagnac-like interferometer satisfies the requirement for atomic spin precession detection on MEG systems. After cutting off the calibrated optical rotation, the optical noise is tested. The optical noise falls slightly with a level of 3.15×10^{-7} rad/Hz$^{1/2}$, which gets rid of the noise induced by the reflective plane of optical

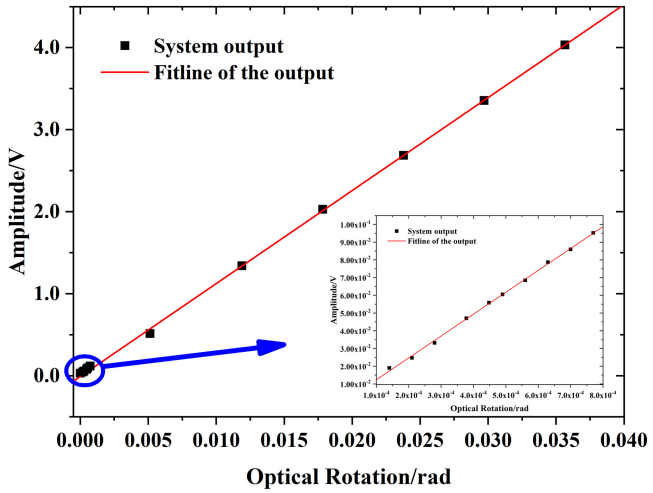

Fig. 8. Measured signal of fiber Interferometer for different input optical rotation. The dots are the experimental results; the red line is the fitted line of the output.

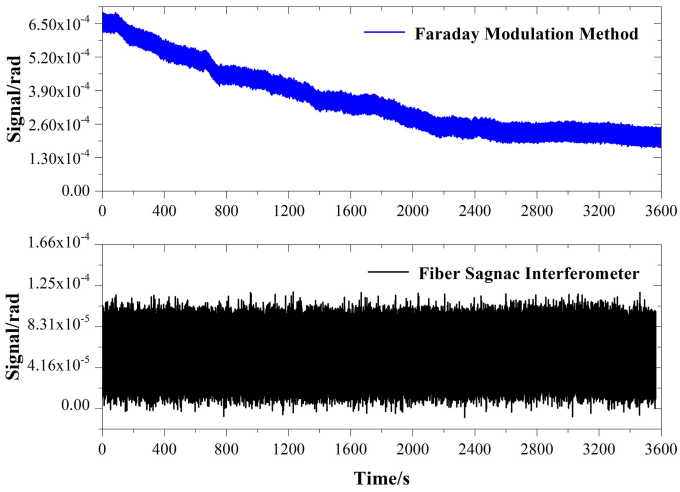

Fig. 9. The output for one hour compared with Faraday modulation method.

rotation generator in free space. Then, the light is blocked and the output is recorded. The results show that the electric noise of the system has a value of 2.19×10^{-7} rad/Hz$^{1/2}$. The system noise satisfies the requirement for MEG system applications. However, the optimization should be focused on the plane of optical elements in free space by titling the planes of free-space optical elements with a small angle.

Fig. 8 shows the system response for different optical rotation inputs ranging within 0–0.036 rad. Within this range, the system outputs stay linear with respect to optical rotation inputs. The measurement range of the fiber system is larger than 0.035 rad, which is far bigger than the optical rotation range for MEG system.

Fig. 9 shows the stability of single-fiber Sagnac-like interferometer for one hour compared with the Faraday modulation method. Both system outputs (without alkali metal vapor) are recorded with the same lock-in amplifier and parameters. Both the systems are calibrated with the same optical rotation input

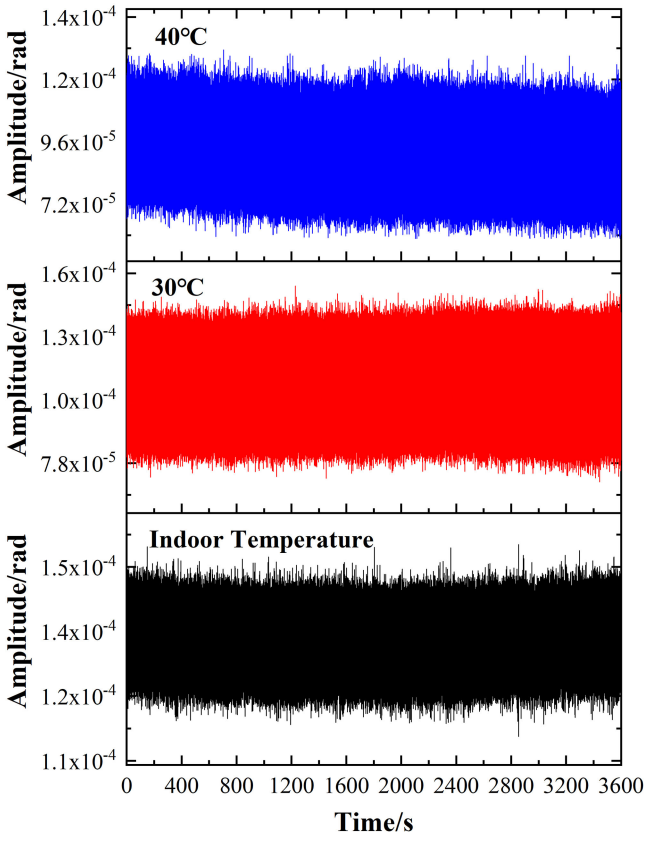

Fig. 10. The output for one hour with different temperature. The black line is the output for one hour with indoor temperature; the red line is the output for one hour with 30 °C; the blue line is the output for one hour with 40 °C.

before the measurement. Although the performance at 30 Hz is more interesting than that at DC for MEG applications, the DC output may be closer to fiber system's intrinsic noise. The results show a distinctly better stability of fiber Sagnac interferometer, which benefits from the reciprocal light path with a variance of 7.76×10^{-7} rad/h, while the Faraday modulation method has the corresponding value of 2.68×10^{-6} rad/h. Moreover, the drift of a commercial atomic magnetometer is about 2 pT/h [16], which is 2×10^{-4} rad/h. Compared with the proposed system, the results shown in Fig. 9 show that the drift of fiber system is much better than the requirement of atomic magnetometer, while the drift of Faraday modulation method is only 3.8×10^{-4} rad/h.

Fig. 10 shows the system output for one hour against the indoor temperatures of 30 °C and 40 °C. The variance of single-fiber Sagnac-like interferometer stays at the level of 1×10^{-4} rad/h at different temperatures. However, the signal decreases with the increase in temperature, which increases the attenuation of fiber nonlinearly. If the environment has enormous temperature differences, the system should be re-calibrated. In such a case, some special optical fibers, such as crystal fiber, should be considered to tackle these environmental variations.

Fig. 11 shows the system output for 5 min against different bending radii of the single-fiber Sagnac-like interferometer. The bending position of the fiber is chosen after phase modulator. For

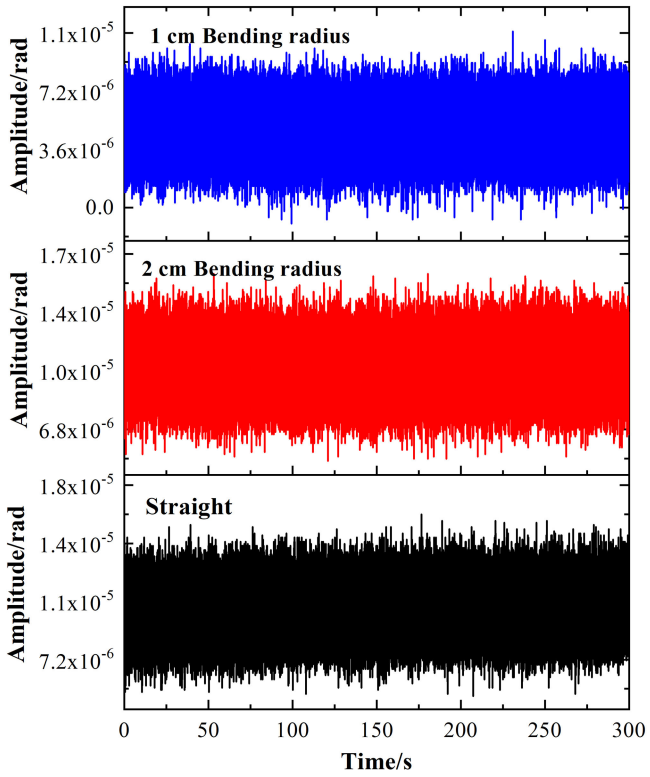

Fig. 11. The output for one hour with different bending radius; the black line is for system without bending; the red one is for bending radius of 2 cm; the blue one is for bending radius of 1 cm.

2 cm, 1 cm and no bending radius, the system has a smooth and steady output with the variance level of 10^{-11} rad/min. However, the signal attenuates with the decrease in bending radius as the optical attenuation increases with the radius.

V. Conclusion

In this work, an atomic spin precession detection method, which is based on single-fiber Sagnac-like interferometer, is demonstrated. Preliminary experiments achieved noise limited detection sensitivities of 2.6 pT/Hz$^{1/2}$ with an SLD source and 11.1 pT/Hz$^{1/2}$ with a laser source. The single-fiber Sagnac-like interferometer produced satisfactory performance for applications in MEG systems with an equivalent magnetic sensitivity of 3.49 fT/Hz$^{1/2}$. The structure of single-fiber Sagnac-like interferometer enables a more compact and flexible sensing header for remote measurement and a capacity of higher spatial resolution MEG system. In addition, the reciprocity of the single-fiber Sagnac-like interferometer guarantees insensitivity to environmental disturbances, which has nearly an order of magnitude improvement for one-hour stability compared to Faraday modulation method. Moreover, the system also reveals satisfactory performance under thermal and bending disturbances. However, the use of a low coherence SLD probe source greatly reduces the coherent backscattering noise and also reduces the signal amplitude to a certain extent. Further optimization of the probe source is possible to achieve better detection sensitivity.

References

[1] M. W. Evans, "New field-induced axial and circular birefringence effects," *Phys. Rev. Lett.*, vol. 64, no. 24, pp. 2909–2912, 1990.

[2] C. Patterson, M. Syed, and Y. Takemura, "Harmonic decomposition of magneto-optical signal from suspensions of superparamagnetic nanoparticles," *J. Magn. Magn. Mater.*, vol. 451, pp. 248–253, 2018.

[3] M. Villiger *et al.*, "Repeatability assessment of intravascular polarimetry in patients," *IEEE Trans. Med. Imag.*, vol. 37, no. 7, pp. 1618–1625, Jul. 2018.

[4] C. Johnson, P. D. D. Schwindt, and M. Weisend, "Magnetoencephalography with a two-color pump-probe, fiber-coupled atomic magnetometer," *Appl. Phys. Lett.*, vol. 97, no. 24, pp. 413–375, 2010.

[5] D. Budker *et al.*, "Resonant nonlinear magneto-optical effects in atoms," *Rev. Mod. Phys.*, vol. 74, no. 4, pp. 1153–1201, 2002.

[6] A. P. Colombo *et al.*, "Four-channel optically pumped atomic magnetometer for magnetoencephalography," *Opt. Express*, vol. 24, no. 14, pp. 15403–15416, 2016.

[7] H. B. Dang, A. C. Maloof, and M. V. Romalis, "Ultrahigh sensitivity magnetic field and magnetization measurements with an atomic magnetometer," *Appl. Phys. Lett.*, vol. 97, no. 15, 2010, Art. no. 151110.

[8] R. Wyllie, M. Kauer, G. S. Smetana, R. T. Wakai, and T. G. Walker, "Magnetocardiography with a modular spin-exchange relaxation-free atomic magnetometer array," *Phys. Med. Biol.*, vol. 57, no. 9, pp. 2619–2632, 2012.

[9] S. J. Seltzer and M. V. Romalis, "Unshielded three-axis vector operation of a spin-exchange-relaxation-free atomic magnetometer," *Appl. Phys. Lett.*, vol. 85, no. 20, pp. 4804–4806, 2004.

[10] W. Happer and B. S. Mathur, "Off-resonant light as a probe of optically pumped alkali vapors," *Phys. Rev. Lett.*, vol. 18, 1967, Art. no. 577.

[11] H. Xia *et al.*, "Magnetoencephalography with an atomic magnetometer," *Appl. Phys. Lett.*, vol. 75, no. 21, 2006, Art. no. 211104.

[12] I. K. Kominis, T. W. Kornack, J. C. Allred, and M. V. Romalis, "A subfemtotesla multichannel atomic magnetometer," *Nature*, vol. 422, no. 6932, pp. 596–599, 2003.

[13] E. Boto *et al.*, "Moving magnetoencephalography towards real-world applications with a wearable system," *Nature*, vol. 555, pp. 657–661, 2018.

[14] D. Budker, "Atomic physics—A new spin on magnetometry," *Nature*, vol. 422, no. 6932, pp. 574–575, 2003.

[15] M. A. Kagan and E. A. Khazanov, "Thermally induced birefringence in Faraday devices made from terbium gallium garnet-polycrystalline ceramics," *Appl. Opt.*, vol. 43, no. 32, pp. 6030–6039, 2004.

[16] J. Osborne, J. Orton, O. Alem, and V. Shah, "Fully integrated standalone zero field optically pumped magnetometer for biomagnetism," *Proc. SPIE*, vol. 10548, 2018, Art. no. 105481G.

[17] X. Dong, H. Y. Tam, and P. Shum, "Temperature-insensitive strain sensor with polarization-maintaining photonic crystal fiber based Sagnac interferometer," *Appl. Phys. Lett.*, vol. 90, no. 15, 2007, Art. no. 151113.

[18] T. Wei, Y. Han, Y. Li, H. Tsai, and H. Xiao, "Temperature-insensitive miniaturized fiber inline Fabry-Perot interferometer for highly sensitive refractive index measurement," *Opt. Express*, vol. 16, no. 8, pp. 5764–5769, 2008.

[19] Y. Gong, T. Zhao, Y. J. Rao, and Y. Wu, "All-fiber curvature sensor based on multimode interference," *IEEE Photon. Technol. Lett.*, vol. 23, no. 11, pp. 679–681, Jun. 2011.

[20] L. Li, L. Xia, Z. Xie, and D. Liu, "All-fiber Mach-Zehnder interferometers for sensing applications," *Opt. Express*, vol. 20, no. 10, pp. 11109–11120, 2012.

[21] Z. Tian, S. S. H. Yam, and H. P. Loock, "Refractive index sensor based on an abrupt taper Michelson interferometer in a single-mode fiber," *Opt. Lett.*, vol. 33, no. 10, pp. 1105–1107, 2008.

[22] H. Hirsch and D. Peier, "Linearization of fiber-optic polarimetric current sensors," *Opt. Commun.*, vol. 82, no. 3, pp. 193–196, 1991.

[23] J. Blake, P. Tantaswadi, and R. T. De Carvalho, "In-line Sagnac interferometer current sensor," *IEEE Trans. Power Del.*, vol. 11, no. 1, pp. 116–121, Jan. 1996.

[24] V. Budinski and D. Donlagic, "Miniature all-fiber rotation sensor based on temperature compensated wave plate," *IEEE Photon. Technol. Lett.*, vol. 27, no. 1, pp. 85–88, Jan. 2015.

[25] R. C. Jones, "A new calculus for the treatment of optical systems I. Description and discussion of the calculus," *J. Opt. Soc. Amer.*, vol. 31, no. 7, pp. 488–493, 1941.

[26] K. Hotate and K. Tabe, "Drift of an optical fiber gyroscope caused by the Faraday effect: Influence of the earth's magnetic field," *Appl. Opt.*, vol. 25, no. 7, pp. 1086–1092, 1986.

[27] J. C. Allred, R. N. Lyman, T. W. Kornack, and M. V. Romalis, "High-sensitivity atomic magnetometer unaffected by spin-exchange relaxation," *Phys. Rev. Lett.*, vol. 89, no. 13, 2002, Art. no. 130801.
[28] S. J. Seltzer, "Developments in alkali-metal atomic magnetometry," Ph.D. dissertation, Dept. Phys., Princeton Univ., Princeton, NJ, USA, 2008.
[29] M. P. Ledbetter, I. M. Savukov, V. M. Acosta, D. Budker, and M. V. Romalis, "Spin-exchange relaxation free magnetometry with Cs vapor," *Phys. Rev. A*, vol. 77, no. 3, pp. 1012–1015, 2007.
[30] J. Sheng *et al.*, "Magnetoencephalography with a Cs-based high-sensitivity compact atomic magnetometer," *Rev. Sci. Instrum.*, vol. 88, no. 9, 2017, Art. no. 094304.
[31] V. Shah and M. Romalis, "Spin-exchange-relaxation-free magnetometry using elliptically-polarized light," *Phys. Rev. A*, vol. 80, 2009, Art. no. 013416.
[32] J. Fang *et al.*, "In situ magnetic compensation for potassium spin-exchange relaxation-free magnetometer considering probe beam pumping effect," *Rev. Sci. Instrum.*, vol. 85, no. 6, 2014, Art. no. 063108.
[33] S. Zou *et al.*, "Ultra-sensitive atomic magnetometer for studying magnetization fields produced by hyperpolarized helium-3," *J. Appl. Phys.*, vol. 119, no. 14, 2016, Art. no. 143901.
[34] K Böhm, P. Russer, E. Weidel, and R. Ulrich, "Low-noise fiber-optic rotation sensing," *Opt. Lett.*, vol. 6, no. 2, pp. 64–66, 1981.

Xuejing Liu received the B.E. degree in optic electronics from Yanshan University, Qinhuangdao, China, in 2011. She is currently working toward the Ph.D. degree with Beihang University, Beijing, China. Her current research interest is the fiber sensors for atomic magnetometer applications.

Yuanhong Yang received the Ph.D. degree from Beihang University, Beijing, China, in 2004. He is currently a Professor and a Ph.D. Supervisor with the School of Photoelectric Research, Beihang University, Beijing, China. His research interests include optical fiber gyroscope, photoelectron device, and distributed optical fiber sensing technology.

Ming Ding received the Ph.D. degree in optoelectronics from the Optical Fiber Nanowires and Related Devices Group, Optoelectronics Research Centre, University of Southampton, Southampton, U.K., in 2013. She is currently a Professor with the International Research Institute for Multidisciplinary Science, Beihang University, Beijing, China.

Wei Quan received the Ph.D. degree in precision instruments and machinery from Beihang University, Beijing, China, in 2008. He is currently a Professor and a Ph.D. Supervisor with Beihang University. His research interests include atomic serf gyro, multisensor integrated navigation, and quantum precision measurement.

Yanhui Hu received the B.Sc. degree in applied physics from Beijing Institute of Technology, Beijing, China in 2015, and the M.Sc. degree in instrumentation science and technology from Beihang University, Beijing, in 2018. His current research interests include opto-electronics, and optical sensors and devices.

Yang Li received the B.E. degree in applied physics from Beihang University, Beijing, China, in 2011. He is currently working toward the Ph.D. degree in Beihang University. His current research interest is the hybrid optical pumping atomic magnetometer.

Wei Jin received the Ph.D. degree in optical fiber from Strathclyde University, Glasgow, U.K., in 1991. He is currently a Professor with the Department of Electrical Engineering, Hong Kong Polytechnic University, Hong Kong. His research interests include fiber sensing, photonic crystal fiber theory, fiber gas sensing technology, and fiber grating sensing technology.

Jiancheng Fang received the Ph.D. degree in measurement technology and instruments from Southeast University, Nanjing, China, in 1996. He is currently a Member of Chinese Academy of Sciences and the Vice-Principal of Beihang University, Beijing, China. His research interests include atomic magnetometer, inertia navigation, and Maglev motor technology.